Direct-write Nanocomposite Sensor Array for Ultrasonic Imaging of Composites

Pengyu Zhou[a‡], Xiongbin Yang[a‡], Yiyin Su[a], Jianwei Yang[a], Lei Xu[a],

Kai Wang[b], Li-min Zhou[c] and Zhongqing Su[a,d,e]*

[a] Department of Mechanical Engineering,

The Hong Kong Polytechnic University, Kowloon, Hong Kong SAR

[b] Department of Aeronautical and Aviation Engineering,

The Hong Kong Polytechnic University, Kowloon, Hong Kong SAR

[c] School of System Design and Intelligent Manufacturing,

Southern University of Science and Technology, Shenzhen 518055, PR China

[d] The Hong Kong Polytechnic University Shenzhen Research Institute,

Shenzhen 518057, PR China

[e] School of Astronautics,

Northwestern Polytechnical University, Xi'an 710072, PR China

[‡] These authors contributed equally.

[*] To whom correspondence should be addressed. Tel.: +852-2766-7818, Fax: +852-2365-4703,
Email: zhongqing.su@polyu.edu.hk (Prof. Zhongqing Su, *Ph.D.*)

28   **Abstract**

29   To improve the ultrasonic imaging of composites, an all-printed nanocomposite sensor array

30   (APNSA) is developed using a direct-write approach. Individual sensing elements of

31   APNSA are inkjet printed by directly writing graphene/poly (amic acid) (PAA)-based

32   nanocomposite ink on Kapton film substrates, with an ultra-thin thickness of ~ 1 μm only.

33   APNSA is morphologically tuned at a nano scale to be sensitive to acousto-ultrasonic waves

34   of a broad band regime. Each sensing element features a homogenous and consolidated

35   nanostructure, with which transient change of tunneling resistance between adjacent

36   graphene nanoplatelets in the polyimide (PI) matrix can be triggered when the element is

37   loaded with acousto-ultrasonic waves. The triggered quantum tunneling effect endows

38   APNSA with capability to perceive dynamic strains in a broadband regime with high fidelity

39   and accuracy. Compared with a conventional ultrasonic phased array which is of a low

40   degree of compatibility with composites, APNSA can be fully integrated with the inspected

41   composites. In conjunction with the use of the additively manufactured APNSA, ultrasonic

42   imaging of composites can be implemented, spotlighting a nature of full integration of

43   APNSA with composites for *in situ* structural health monitoring and anomaly detection, yet

44   without degrading the original integrity of the composites.

45

46   *Keywords*: Nanocomposite sensor array; Additive manufacturing; Ultrasonic imaging;

47   Composites structural health monitoring

1. Introduction

With the ability of directional scanning and high-precision signal acquisition, phased array technique has secured its popularity in radar searching [1], sonar positioning [2], seismology study [3], telecommunication [4], and biomedical imaging [5], as well as non-destructive testing (NDT) [6, 7]. Particularly for NDT, with multiple, synchronized sensing elements, a phased array features merits including wave focusing, steerable inspection and enhanced signal-to-noise ratio, through which a broad region can be scanned, and rich information on material defect or structural anomaly can be obtained.

Despite proven effectiveness when used for ultrasonic imaging of composite structure [8], conventional ultrasonic phased arrays are encountering problematic issues. With a bulky and unwieldy nature, phased arrays are of a low degree of coupling compatibility with inspected structure [9], limited adaptation to curved or geometrically complex structural surfaces [10], possible blind zones [11], and low inspection efficiency due to the need of manipulating arrays back and forth along the inspected surface. In particular, the impossibility of integrating an array with the inspected structure precludes the phased array-based inspection from being extended from offline NDT to *in situ*, real-time ultrasonic imaging of composite structure.

In the past decade, additive manufacturing has paved a promising way to develop innovative electronics and devices [12-14], including sensing devices [15], transistors [16], flexible radio frequency identification (RFID) [17] and battery electrodes [18], to name a few. Amongst appealing additive manufacturing techniques, direct-write inkjet printing, by directly depositing functional inks onto various substrates, has gained prominence towards electronic device fabrication in a large-scale and cost-effective manner. With its high

73   automaticity and controllability, direct-write inkjet printing warrants ultrahigh fabrication

74   precision, and in the meantime allows the electronics to be tailor-made with specific patterns

75   and functionalities [19].

76

77   In the authors' previous attempts [20-23], nanocomposite-based ultrasonic sensors have been

78   developed, and proven to be applicable to various structures, with advantages including high

79   flexibility, ultralight weight, broadband responsivity (up to frequency of 1.6 MHz), and good

80   sensitivity to ultrasound signals that feature ultra-weak magnitudes (in the order of

81   microstrain or even smaller), along with significantly reduced producing cost. The sensors

82   leverage quantum tunneling effect formed in a nanoparticle-formed percolated network in

83   the sensor [24]. The tunneling effect is triggered when an acousto-ultrasonic wave traverses

84   the sensors, inducing dynamic alteration of tunneling resistance between adjacent electrical-

85   conductive nanofillers and leading to subtle changes in piezoresistivity of the sensors. Thus-

86   produced sensors manifest ultrafast sensing response and excellent sensing accuracy to

87   broadband acousto-ultrasonic waves.

88

89   Recognizing the deficiencies that conventional phased arrays are facing, and extending the

90   authors' continued endeavours in developing nanocomposite-inspired sensors, we develop

91   all-printed nanocomposite sensor array (APNSA) using a direct-write approach. APNSA is

92   fabricated via drop-on-demand inkjet printing, by directly writing graphene/PAA-based

93   nanocomposite ink on Kapton film substrates. With novel graphene/polyimide (PI) sensors

94   as individual sensing elements and by virtue of the quantum tunneling effect, APNSA is

95   functionalized to substitute conventional ultrasonic phased array which is of a low degree of

96   integrity with composites, for acquiring acousto-ultrasonic waves and implementing *in situ*

97   ultrasonic imaging of composites.

98

2. Results and Discussion

Individual sensing elements of APNSA are inkjet printed by directly writing graphene/poly (amic acid) (PAA)-based nanocomposite sensing ink on a Kapton film substrate. Details of graphene/PAA sensing ink and APNSA fabrication, morphological characterization, and acousto-ultrasonic wave responsivity calibration are elaborated in the Supplementary Material. The graphene/PI sensing elements of APNSA show a homogenous and consolidated nanostructure (**Figures 1(a)** and **(b)**) and feature an ultra-thin thickness of ~ 1 μm only (**Fig. S1**). Benefiting from this, the charge carriers of neighbouring graphene nanoplatelets are able to pass through the potential barrier, when the sensing element is loaded with an acousto-ultrasonic wave even with an ultra-low magnitude. This triggers the quantum tunneling effect that further alters the tunneling resistance between neighbouring graphene nanoplatelets, in pace with the acousto-ultrasonic wave. Such a transient variation of tunneling condition in the percolation network leads to the consequent change in piezoresistivity of each sensing element of APNSA, endowing the sensing elements with prominent capability for acquisition of broadband acousto-ultrasonic wave signals (**Figs. S3**, **S4** and **S5**). The number of sensing elements in an APNSA depends on specific applications, and a paradigm of an APNSA with 12 sensing elements deployed on Kapton film is pictured in **Fig. 1(c)**.

117
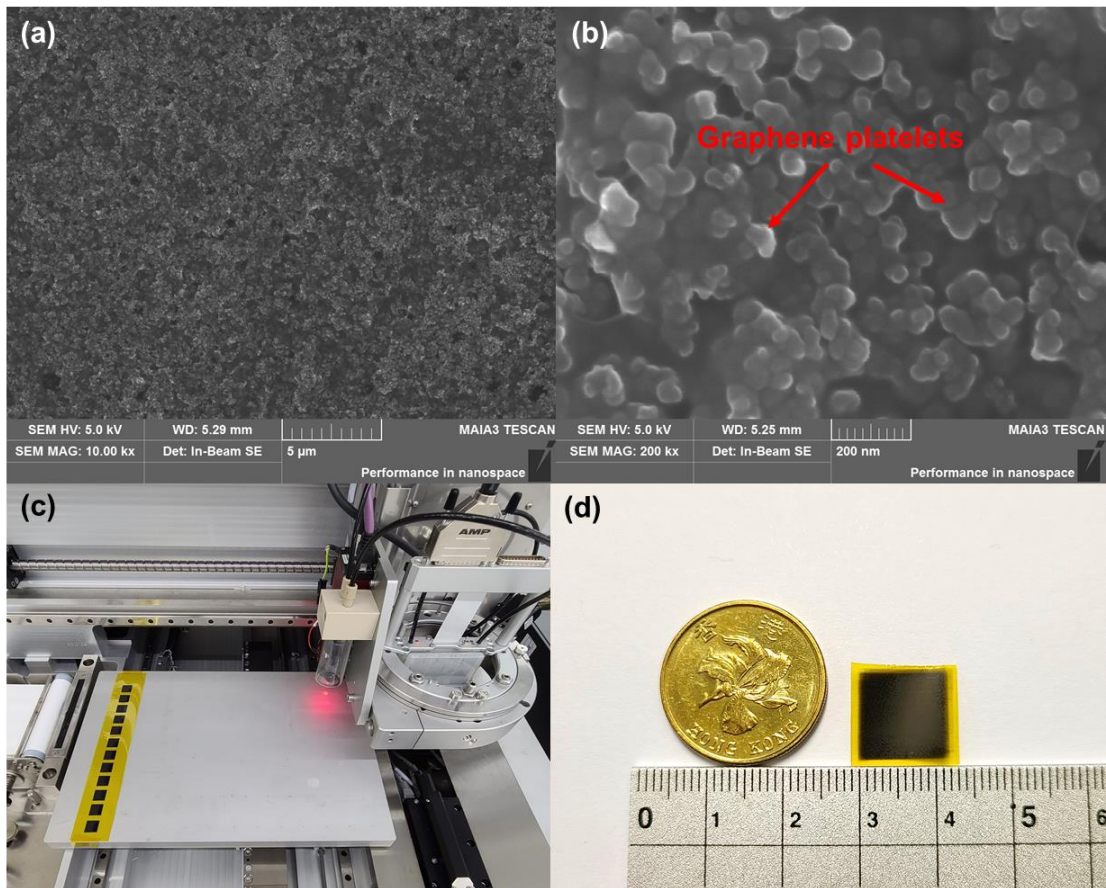
Fig. 1. Field emission scanning electron microscope (FESEM) image of graphene/PI sensing element of APNSA: (a) 10.00 k× magnification; and (b) 200 k× magnification; (c) APNSA on a Kapton film substrate, printed on a desktop inkjet printing platform; and (d) a typical graphene/PI sensing element of an APNSA.

With proven responsivity and sensing precision in responding to broadband acousto-ultrasonic wave signals, the fabricated APNSA is applied to implement *in situ* ultrasonic imaging for a glass fibre/epoxy composite laminate plate, pictured in **Fig. 2(a)**, as a proof-of-concept validation. An APNSA consisting of eight graphene/PI sensing elements (labelled as S1, S2, …, S8) is surface-mounted on the plate, and a piezoelectric lead zirconate titanate (PZT) wafer (Ø12 mm, 1 mm thick) is mounted on the plate surface as a wave actuator. The locations of the APNSA and PZT wafer on the plate are indicated in **Fig. 2(b)**. A steel cylinder (Ø20 mm, 200 g weight) is bonded on the plate as a mock-up anomaly, at the

132   location of (30 mm, 10 mm), in **Fig. 2(b)**. The experimental system and measurement

133   procedures remain the same as the responsivity calibration experiment. A five-cycle

134   Hanning-windowed sinusoidal tone-burst at a central frequency of 100 kHz is applied to

135   drive the PZT actuator, to generate a probing wave with wavelength (λ) of 37.2 mm in the

136   laminate. For the APNSA, the shape effect of the sensing element on the sensing responsivity

137   can be considered negligible. The element pitch (*i.e.*, distance between the centres of

138   neighbouring sensing elements, denoted by *l* herein-after) has been pre-set as 16 mm during

139   inkjet printing, which is smaller than the half wavelength (*i.e.*, 18.6 mm) of the generated

140   probing wave, and this will ensure the detection resolution and avoid false results caused by

141   spatial aliasing [25].

142
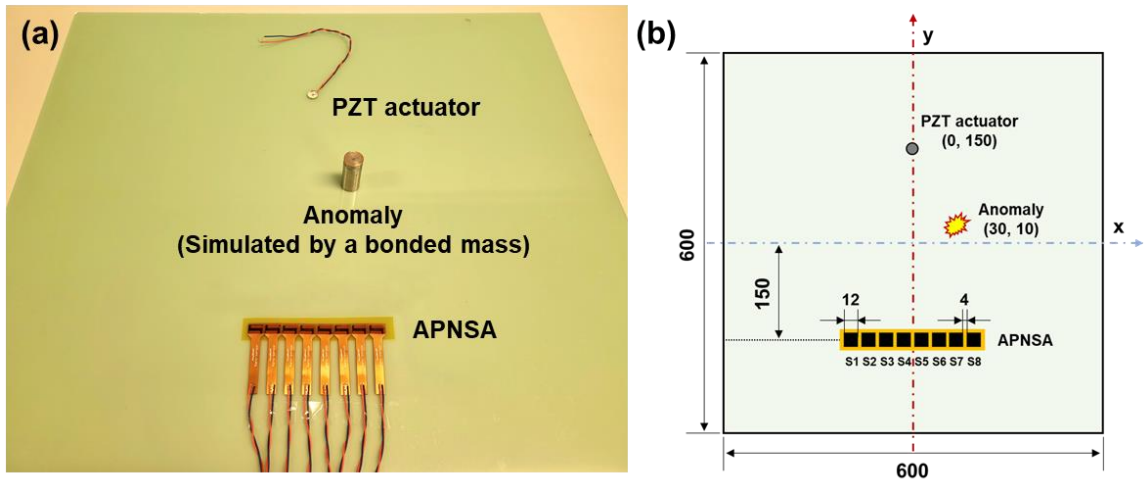
143

144   **Fig. 2.** (a) Photograph and (b) schematic of the glass fibre/epoxy composite laminate plate

145   with APNSA and a mock-up anomaly (unit: mm).

146

147   **Figure 3(a)** presents representative signals captured by sensing element S1 of APNSA,

148   before and after that the mock-up anomaly is introduced to the laminate plate. The S_0 (the

149   zeroth-order symmetric plate wave mode guided by the laminate) wave mode of the probing

150   wave can be perceived clearly in both cases. After introducing the mock-up anomaly, an

151　additional wave packet, following the original S_0 mode, is prominent which is classified as

152　the anomaly-induced wave component in the sensing element-captured signal [26, 27]. For

153　anomaly imaging, this additional wave component is extracted, **Fig. 3(b)**, and named the

154　anomaly-scattered S_0 mode ($S_0^{Anomaly}$).

155
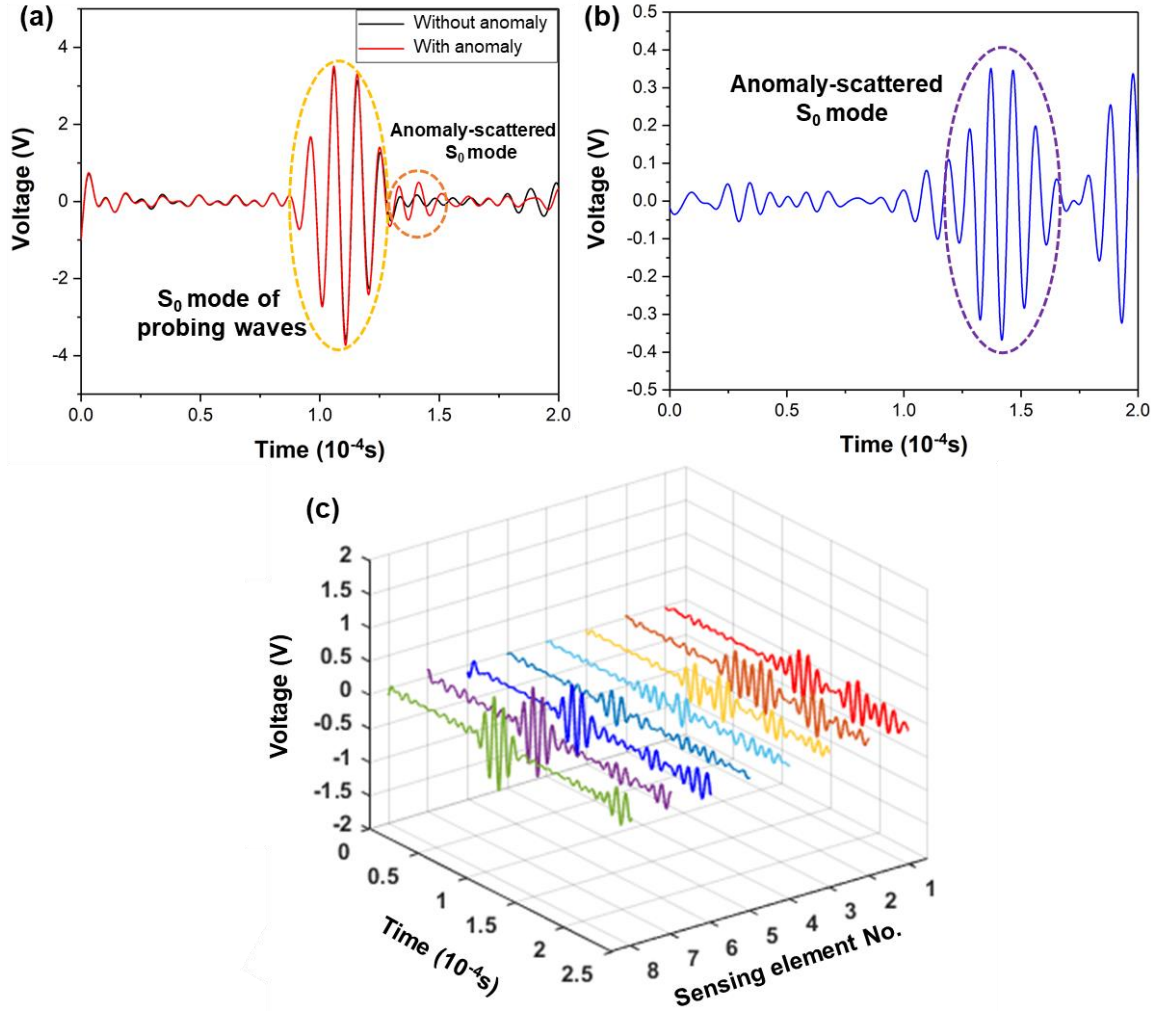
156

157

158　**Fig. 3.** (a) Wave signals captured by S1 of APNSA, before and after the mock-up anomaly

159　introduced; (b) $S_0^{Anomaly}$ in the signal captured by S1; and (c) $S_0^{Anomaly}$ in signals captured by

160　all the sensing elements of APNSA.

161

162   Analogously, the $S_0^{Anomaly}$ is in turn extracted from the signal captured by each sensing

163   element of APNSA, as shown in **Fig. 3(c)**. The *multiple signal classification* (MUSIC) – an

164   array signal processing method for ultrasonic imaging [28, 29], is applied (**Fig. 4**). As

165   indicated in **Fig. 4**, the actuator is placed at position (x_0, y_0), and the mth sensing element of

166   APNSA (Sm, $m = 1, 2, \ldots, 8$) is located at (x_m, y_m). All extracted $S_0^{Anomaly}$ are written as a

167   matrix form [30], as

$$\boldsymbol{R}^{S_0^{Anomaly}}(t) = [r_1(t),\ldots,r_m(t),\ldots,r_8(t)]^{\mathrm{T}}, \tag{1}$$

168   where $\boldsymbol{R}^{S_0^{Anomaly}}(t)$ denotes the matrix of $S_0^{Anomaly}$ acquired by all elements of APNSA, and

169   $r_m(t)$ signifies $S_0^{Anomaly}$ captured via the mth sensing element. Assuming that a scanning

170   position in the inspection region is at (x, y), the APNSA steering vector $A(x, y)$ at this position

171   can be defined as

$$A(x, y) = [a_1(x, y),\ldots,a_m(x, y),\ldots,a_8(x, y)], \tag{2}$$

172   where

$$a_m(x, y) = e^{j\omega_0 \tau_m}, \tag{3}$$

$$\tau_m = \frac{d_1 - d_m}{c}, \quad (m = 1, 2, \ldots, 8) \tag{4}$$

$$d_m = \sqrt{(x_0 - x)^2 + (y_0 - y)^2} + \sqrt{(x - x_m)^2 + (y - y_m)^2}. \tag{5}$$

173   In Eqs. (3)-(5), $a_m(x, y)$ is the steering vector of sensing element Sm, and τ_m is the difference

174   in propagation time between two signals captured by sensing element S1 and element Sm.

175   d_m signifies the wave propagation distance from the actuator to the scanning position, and

176   then to Sm. c is the propagation velocity of the probing waves with central frequency of ω_0.

177
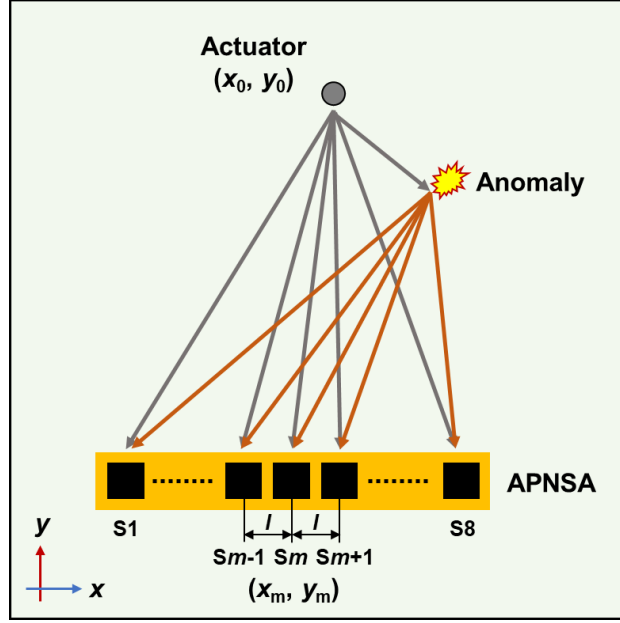
**Fig. 4.** Use of MUSIC algorithm and APNSA for anomaly imaging.

The covariance matrix of the array signals $\boldsymbol{R}^{S_0^{\text{Anomaly}}}(t)$ can be decomposed into signal subspace $\boldsymbol{U}_S$ and noise subspace $\boldsymbol{U}_N$ via an eigenvalue decomposition. Based on the orthogonality between these two subspaces, the pixel value of the spatial spectrum at (x, y), $P_{\text{MUSIC}}(x, y)$, is formulated as

$$P_{\text{MUSIC}}(x, y) = \frac{1}{\boldsymbol{A}^H(x, y)(\boldsymbol{U}_N \boldsymbol{U}_N^H)\boldsymbol{A}(x, y)}. \tag{6}$$

Superscript H represents the complex conjugate transpose. By varying the scanning position (x, y), the spatial spectrum of the entire inspection region of the laminate is obtained. When the scanning position matches the anomaly location, the steering vector $\boldsymbol{A}(x, y)$ is orthogonal with regard to the noise subspace $\boldsymbol{U}_N$, and thus the denominator of Eq. (6) approaches 0, resulting in a peak in the spatial spectrum that corresponds to the anomaly location. The anomaly imaging result is shown in **Fig. 5**: the area with highest field value suggests the location of the mock-up anomaly, which shows high coincidence with the true location,

192 demonstrating the great application potential of the developed APNSA towards *in situ*

193 composite structural health monitoring.

194
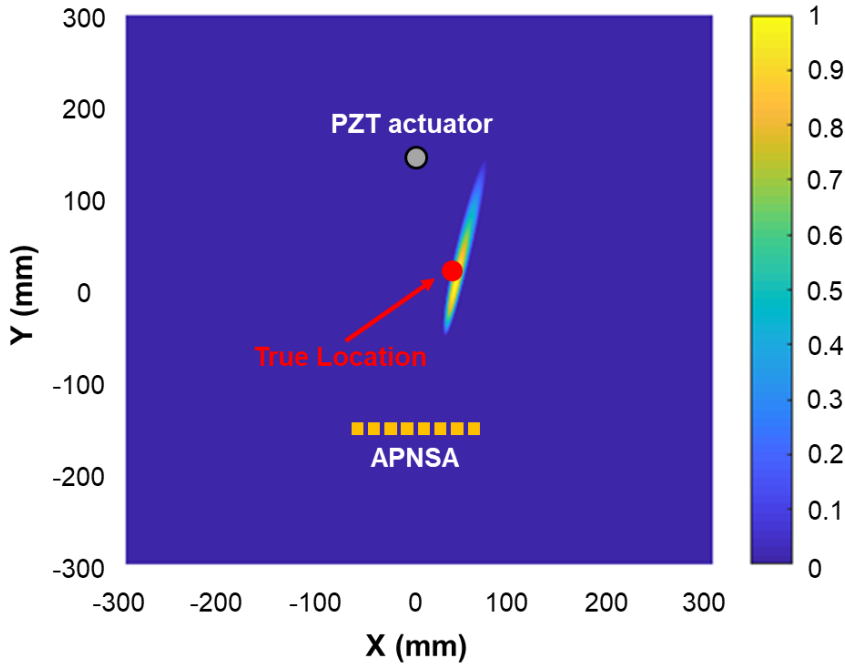
195

196 **Fig. 5.** Anomaly image obtained via MUSIC algorithm and APNSA.

197

198 **3. Conclusions**

199 The nanocomposite-based APNSA is developed, and fabricated via a direct-write additive

200 manufacturing approach. Leveraging graphene/PAA-based nanocomposite sensing ink,

201 novel graphene/PI sensors, as individual sensing elements of APNSA, are inkjet printed on

202 Kapton film substrates, with an ultra-thin thickness of ~ 1 μm only and a homogenous and

203 consolidated nanostructure. When acousto-ultrasonic waves traverse APNSA, transient

204 change of tunneling resistance between adjacent graphene nanoplatelets in the PI polymeric

205 matrix is triggered, endowing APNSA with ultra-sensitive responsivity to dynamic strains in

206 a broadband regime. APNSA can be fully integrated with the inspected composite structure,

207 without degrading its original structural integrity – a task that is challenging to be fulfilled

11

using conventional ultrasonic phased arrays. With a high degree of compatibility with the host structure, the APNSA manifests proven effectiveness in performing anomaly imaging of composite laminates, in lieu of conventional ultrasonic phased arrays with insufficient structural compatibility, limited surface adaptation, and low inspection efficiency, highlighting its alluring application prospects towards *in situ* structural health monitoring of composites.

References

[1] C. Wang, M. Chen, H. Lei, K. Yao, H. Li, W. Wen, D. Fang, Radar stealth and mechanical properties of a broadband radar absorbing structure, Composites Part B: Engineering 123 (2017) 19-27.

[2] X. Pan, J. Jiang, N. Wang, Evaluation of the performance of the distributed phased-MIMO sonar, Sensors 17(1) (2017) 133.

[3] M.M. Huda, C.A. Langston, Coherence and variability of ground motion in New Madrid Seismic Zone using an array of 600 m, Journal of Seismology 25 (2021) 433-448.

[4] D. Blanco, E. Rajo-Iglesias, A.M. Benito, N. Llombart, Leaky-wave thinned phased array in PCB technology for telecommunication applications, IEEE Transactions on Antennas and Propagation 64(10) (2016) 4288-4296.

[5] A. Cebrecos, J.J. García-Garrigós, A. Descals, N. Jiménez, J.M. Benlloch, F. Camarena, Beamforming for large-area scan and improved SNR in array-based photoacoustic microscopy, Ultrasonics 111 (2021) 106317.

[6] X. Lei, H. Wirdelius, A. Rosell, Experimental validation of a phased array probe model in ultrasonic inspection, Ultrasonics 108 (2020) 106217.

237 [7] X. Yang, K. Wang, Y. Xu, L. Xu, W. Hu, H. Wang, Z. Su, A reverse time migration-
238 based multistep angular spectrum approach for ultrasonic imaging of specimens with
239 irregular surfaces, Ultrasonics 108 (2020) 106233.

240 [8] Z. Zhang, M. Liu, Q. Li, Y. Ang, Visualized characterization of diversified defects in
241 thick aerospace composites using ultrasonic B-scan, Composites Communications 22 (2020)
242 100435.

243 [9] J. Brizuela, J. Camacho, G. Cosarinsky, J.M. Iriarte, J.F. Cruza, Improving elevation
244 resolution in phased-array inspections for NDT, NDT & E International 101 (2019) 1-16.

245 [10] W. Nsengiyumva, S. Zhong, J. Lin, Q. Zhang, J. Zhong, Y. Huang, Advances,
246 limitations and prospects of nondestructive testing and evaluation of thick composites and
247 sandwich structures: A state-of-the-art review, Composite Structures 256 (2021) 112951.

248 [11] Q. Huan, M. Chen, F. Li, A high-sensitivity and long-distance structural health
249 monitoring system based on bidirectional SH wave phased array, Ultrasonics 108 (2020)
250 106190.

251 [12] Z. Lv, X. Huang, D. Fan, P. Zhou, Y. Luo, X. Zhang, Scalable manufacturing of
252 conductive rubber nanocomposites with ultralow percolation threshold for strain sensing
253 applications, Composites Communications 25 (2021) 100685.

254 [13] B. Li, L. Zhang, B. Yang, Grain refinement and localized amorphization of additively
255 manufactured high-entropy alloy matrix composites reinforced by nano ceramic particles via
256 selective-laser-melting/remelting, Composites Communications 19 (2020) 56-60.

257 [14] S. Lee, Y. Kim, D. Park, J. Kim, The thermal properties of a UV curable acrylate
258 composite prepared by digital light processing 3D printing, Composites Communications 26
259 (2021) 100796.

260 [15] P. Zhou, Y. Liao, Y. Li, D. Pan, W. Cao, X. Yang, F. Zou, L.-m. Zhou, Z. Zhang, Z.
261 Su, An inkjet-printed, flexible, ultra-broadband nanocomposite film sensor for in-situ
262 acquisition of high-frequency dynamic strains, Composites Part A: Applied Science and
263 Manufacturing 125 (2019) 105554.

264 [16] S. Chung, K. Cho, T. Lee, Recent progress in inkjet-printed thin-film transistors,
265 Advanced Science 6(6) (2019) 1801445.

266 [17] R. Singh, E. Singh, H.S. Nalwa, Inkjet printed nanomaterial based flexible radio
267 frequency identification (RFID) tag sensors for the internet of nano things, RSC Advances
268 7(77) (2017) 48597-48630.

269 [18] T.-T. Huang, W. Wu, Scalable nanomanufacturing of inkjet-printed wearable energy
270 storage devices, Journal of Materials Chemistry A 7(41) (2019) 23280-23300.

271 [19] S. Clifton, B.H.S. Thimmappa, R. Selvam, B. Shivamurthy, Polymer nanocomposites
272 for high-velocity impact applications-A review, Composites Communications 17 (2020) 72-
273 86.

274 [20] Z. Zeng, M. Liu, H. Xu, Y. Liao, F. Duan, L.-m. Zhou, H. Jin, Z. Zhang, Z. Su, Ultra-
275 broadband frequency responsive sensor based on lightweight and flexible carbon
276 nanostructured polymeric nanocomposites, Carbon 121 (2017) 490-501.

277 [21] P. Zhou, W. Cao, Y. Liao, K. Wang, X. Yang, J. Yang, Y. Su, L. Xu, L.-m. Zhou, Z.
278 Zhang, Z. Su, Temperature effect on all-inkjet-printed nanocomposite piezoresistive sensors
279 for ultrasonics-based health monitoring, Composites Science and Technology 197 (2020)
280 108273.
281 [22] Y. Su, L. Xu, P. Zhou, J. Yang, K. Wang, L.-m. Zhou, Z. Su, Carbon nanotube-
282 decorated glass fibre bundles for cure self-monitoring and load self-sensing of FRPs,
283 Composites Communications 27 (2021) 100899.
284 [23] P. Zhou, Y. Liao, X. Yang, Y. Su, J. Yang, L. Xu, K. Wang, Z. Zeng, L.-m. Zhou, Z.
285 Zhang, Z. Su, Thermally stable, adhesively strong graphene/polyimide films for inkjet
286 printing ultrasound sensors, Carbon 184 (2021) 64-71.
287 [24] Y. Li, K. Wang, Z. Su, Dispersed sensing networks in nano-engineered polymer
288 composites: from static strain measurement to ultrasonic wave acquisition, Sensors 18(5)
289 (2018) 1398.
290 [25] V. Giurgiutiu, Chapter 13 - In situ phased arrays with piezoelectric wafer active sensors,
291 in: V. Giurgiutiu (Ed.), Structural health monitoring with piezoelectric wafer active sensors
292 (Second Edition), Academic Press, Oxford, 2014, pp. 707-805.
293 [26] K. Wang, Z. Su, Analytical modeling of contact acoustic nonlinearity of guided waves
294 and its application to evaluating severity of fatigue damage, Proc. SPIE 9805, Health
295 Monitoring of Structural and Biological Systems 2016, 98050L.
296 [27] K. Wang, M. Liu, Z. Su, S. Yuan, Z. Fan, Analytical insight into "breathing" crack-
297 induced acoustic nonlinearity with an application to quantitative evaluation of contact cracks,
298 Ultrasonics 88 (2018) 157-167.
299 [28] X. Yang, K. Wang, P. Zhou, L. Xu, J. Liu, P. Sun, Z. Su, Ameliorated-multiple signal
300 classification (Am-MUSIC) for damage imaging using a sparse sensor network, Mechanical
301 Systems and Signal Processing 163 (2022) 108154.
302 [29] Q. Bao, W. Hu, Q. Wang, A novel multi-site damage localization method based on near-
303 field signal subspace fitting using uniform linear sensor array, Ultrasonics 116 (2021)
304 106485.
305 [30] H. Zuo, Z. Yang, C. Xu, S. Tian, X. Chen, Damage identification for plate-like
306 structures using ultrasonic guided wave based on improved MUSIC method, Composite
307 Structures 203 (2018) 164-171.
308